Nano Research

Open Access

Research Article

A color-changing carbon dots/hydrogel composite for human motion sensing and sweat pH detection

Junjie Cai, Huajiang Hu, Jiurong Li, Junfei Liao, and Xiao Gong

State Key Laboratory of Silicate Materials for Architectures, Wuhan University of Technology, Wuhan 430070, China

Cite this article: *Nano Research*, **2025**, *18*, 94907180. https://doi.org/10.26599/NR.2025.94907180

ABSTRACT: Carbon dots (CDs) are a type of fluorescent nanomaterial that have gained significant attention due to their simple synthesis method and excellent optical properties. The unique structure of CDs also allows for effective luminescence tunability. CDs have been reported to be pH-sensitive in many studies. However, most of these reports are based on the variation of the luminescence intensity of CDs with pH change. There are few reports on exploring the linearly tunable variation of the luminescence wavelength with pH value. Hence, we synthesized novel pH-sensitive CDs using a simple solvothermal method. The synthesized CDs can change their luminescence emission wavelength by simply adjusting the pH of the solution. The change in emission wavelength may be due to the alteration in the surface state of the CDs caused by the pH change. This luminous color change of the CDs allows for visual detection of the pH of the solution. In addition, a color-changing hydrogel composite for pH sensing was designed based on the pH sensitivity of the CDs. The CDs@hydrogel has conductive properties that enable it to be used for motion sensing and sweat pH detection.

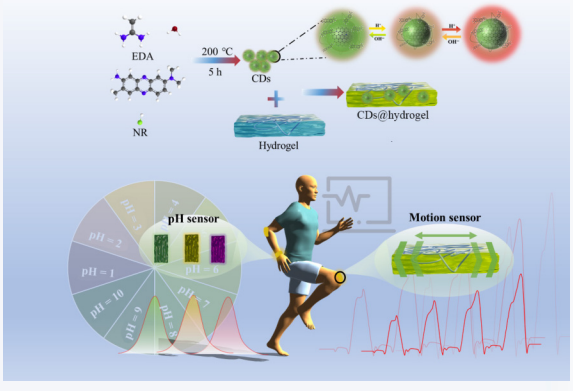

KEYWORDS: carbon dots, multicolor, pH-sensitive, hydrogel, motion sensing

1 Introduction

pH plays an important role in chemical analysis and environmental and physiological processes. Small changes in pH can affect the synthesis and properties of materials, soil stability, water safety, human health, etc. Thus, it is crucial to detect changes in pH. Fluorescent materials are considered to be a popular choice for pH detection, especially carbon dots (CDs), which have recently attracted attention in pH detection [1, 2]. Unfortunately, the use of CDs for pH detection is still quite limited. The majority of pH detections using CDs rely on the pH-induced changes in the luminous intensity of the CDs. However, the luminous intensity can be affected by many factors such as instrumentation [1, 3–6]. Thus, some groups have reported the combined use of more than two fluorescent materials [7–9]. Ratiometric fluorescence sensing, utilizing a range of materials, significantly enhances detection accuracy, although the synthesis process is complicated.

Received: October 4, 2024; **Revised:** December 5, 2024
Accepted: December 11, 2024

Address correspondence to xgong@whut.edu.cn

Hydrogel is a versatile polymeric material with hydrophilic properties and a complex three-dimensional network structure. Hydrogels are formed through chemical (covalent) or physical (non-covalent) cross-linking processes [10–12]. These exceptional materials possess an abundance of hydrophilic groups, enabling them to absorb substantial amounts of water and expand [13]. Due to their cross-linked network and numerous covalent bonds, expanded hydrogels have excellent resistance to dissolution, which allows them to retain absorbed water within the network [10, 14–16]. Additionally, hydrogels feature a porous structure that facilitates the movement of water molecules within the polymer network which allows them to be widely applied in various fields, including engineered skin, medical devices, drug delivery, and wound dressings [16–22]. Various hydrogel sensors have been developed based on factors such as temperature and pH to meet different application requirements in recent years. Notably, the combination of CDs with hydrogels represents a win–win strategy. Compared to single CDs, CD-based hydrogels offer enhanced fluorescence stability by preventing aggregation-induced quenching effects [10, 14, 23]. Furthermore, the incorporation of CDs in CD-functionalized hydrogels introduces luminescent properties that are absent in pure hydrogels, enabling them to fulfill additional functions.

Typically, neutral red (NR) aqueous solution with emission wavelengths located at about 637 nm has pH-independence and is a commonly used acid-base indicator because of its broad absorption band with a peak at 452 nm in alkaline aqueous solution, and its absorption peak shifts to 535 nm under acidic conditions due to rapid deprotonation of acidic NR during photoexcitation or solvent interaction [24, 25]. In this work, one type of new pH-sensitive CDs was reported via using NR and ethylenediamine monohydrate (EDA) as carbon sources (Scheme 1). It is important to note that EDA acts as both a solvent and carbon source, simplifying the synthesis step for CDs. The as-synthesized CDs demonstrate a significant response to changes in pH, as their emission wavelength varies linearly with pH. By precisely adjusting the pH value of the CDs, it can seamlessly transition the emitted light from green to red. This property enables precise determination of the pH value of the solution by measuring the emission wavelength of the CDs, avoiding the inaccuracies and operational complexities of traditional pH determination methods. Additionally, it can be discovered that the emission wavelength change of these CDs causes a significant change in their luminous color, allowing for visual detection of the pH of the solution. Therefore, a novel pH-sensitive luminescent hydrogel (CDs@hydrogel) was successfully prepared by combining pH-sensitive CDs with the hydrogel. This hydrogel inherits the pH sensitivity of the CDs and also exhibits electrical conductivity due to the CDs' electrical conductivity. Ultimately, the as-prepared hydrogels were utilized to sensitively detect human movement and sweat pH.

2 Experimental section

2.1 Chemicals and materials

NR, EDA, ammonium sulfate ($(NH_4)_2SO_4$), phosphate, and sodium hydroxide were purchased from Shanghai Aladdin Biopharmaceutical Co., Ltd. Gelatin (porcine skin) was purchased from Sigma-Aldrich Life Science & Technology Co., Ltd. The pH test paper was purchased from Shanghai SanAiSi Reagent Co., Ltd.

2.2 Synthesis of CDs

CDs were synthesized using a typical solvothermal reaction, i.e., 0.03 g of NR and 1 mL of EDA were weighed and sonicated using an ultrasonic machine for 10 min before using and then the mixture was transferred to an autoclave with a polytetrafluoroethylene liner. The reaction was taken out at 200 °C for 5 h and cooled naturally to obtain the CD solution, which was dialyzed through a dialysis bag with a molecular weight of 1000 Da for 24 h to obtain the purified CDs solution.

2.3 Synthesis of CDs@hydrogel

The gelatin solution was first prepared by dissolving 5 g of gelatin powder in 25 mL of deionized water and stirring at 60 °C for 30 min. When the gelatin was completely dissolved, an appropriate amount of CD solution was added and stirred for 30 min until the CDs were evenly dispersed in the gelatin solution. Subsequently, 1 g of ammonium sulfate was added and the stirring was continued for 30 min, and after removing air bubbles by ultrasonication, the transparent gelatin solution was poured into a polytetrafluoroethylene mold and kept at 4 °C for 1 h to obtain CDs@hydrogel.

2.4 Preparation of CDs@hydrogel sensors

The CDs@hydrogel sensor was obtained by connecting both ends of the hydrogel to a metallic copper wire using conductive copper adhesive and was adhered to the skin using double-sided adhesive when used as human motion sensing. The experiments involving human subjects were performed with the full consent of the participants.

2.5 Characterization

120 KV transmission electron microscopy (TEM) (JEM-2100F) was

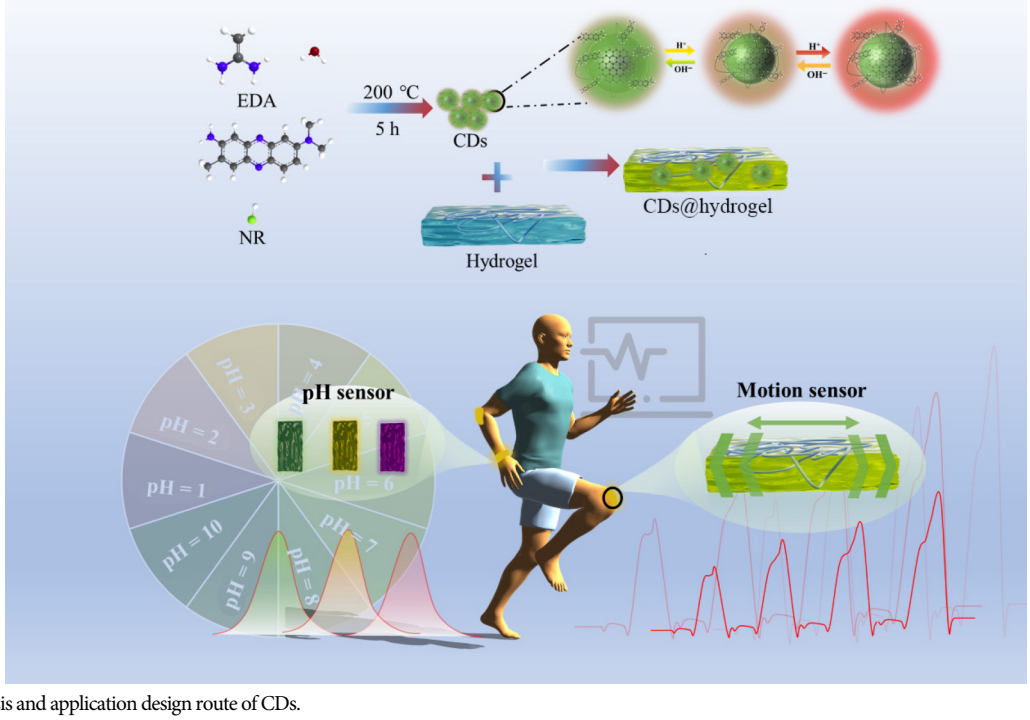

Scheme 1 Synthesis and application design route of CDs.

used for morphology and structure characterization. The surface morphology was characterized by field emission scanning electron microscopy (SEM) (Quanta FEG 450). X-ray photoelectron spectroscopy (XPS) (ESCALAB 250Xi) was utilized for elemental and compositional analysis. X-ray diffraction (XRD) (Bruker, Kα ¼ 1.5406 A) was applied for lattice structure analysis. Fourier transform infrared (FT-IR) spectrometer (Nicolet6700) was utilized for composition and structure analysis. Ultraviolet (UV)–visible near-infrared spectrophotometer (Lambda 750) was used to characterize the optical properties. Photoluminescence (PL) spectra of CDs were measured at room temperature with a time-resolved fluorescence spectrometer (FL3-22, Jobin-Yvon). A benchtop multimeter (NDW3041) was used to measure the resistance of CDs@hydrogel. The static contact angle values of CDs@hydrogel were determined using a droplet shape analyzer (DSA100, Krüss) with a droplet size of 5 μL for each test.

3 Results and discussion

To gain a deeper understanding of the microstructure, size, and distribution of the CDs, we conducted TEM tests. Figure 1(a) shows that the CDs are well dispersed, and TEM reveals that they have a uniform spherical or quasi-spherical distribution. To obtain more accurate size information, we conducted statistical analysis on the particle size of CDs. The results showed that the average particle size of CDs was about 2.13 nm (Fig. 1(b)). The structural details of the CDs reveal obvious lattice stripes (Fig. 1(c)).

The crystal plane spacing of the CDs was measured to be 0.25 nm, corresponding to the (111) crystal plane of graphite, indicating a graphite crystal structure [17]. XRD is a useful tool for reflecting the crystal structure of CDs. The XRD pattern of the CDs shows a wide diffraction peak at approximately 24°, corresponding to the (002) crystal plane of graphite (Fig. 1(d)). To gain a better understanding of the structural information of the CDs, FT-IR analysis was conducted. The FT-IR spectrum of the CDs (Fig. 1(e)) illustrates N–H stretching signals of amines at 3340 and 3220 cm^{-1} [26–28]. The infrared spectrum shows C–H stretching at 2955, 2920, and 2850 cm^{-1}, which may be related to dye molecules [25]. The CDs exhibit a unique C=O bond at 1750 cm^{-1}, which may be due to the oxygen-containing functional groups introduced by the oxidation of the CDs, as confirmed by subsequent XPS analysis [29]. Additionally, the infrared absorption peaks located at 1620, 1585, and 1180 cm^{-1} correspond to the characteristic absorption of C=N, C=C, and C–N bonds, respectively [30–35].

The XPS spectrum is shown in Fig. 1(f), which displays characteristic peaks from C (284.8 eV), N (399.8 eV), and O (532.2 eV). The presence of the O element is indicative of the oxidation of the CDs to produce oxygen-containing functional

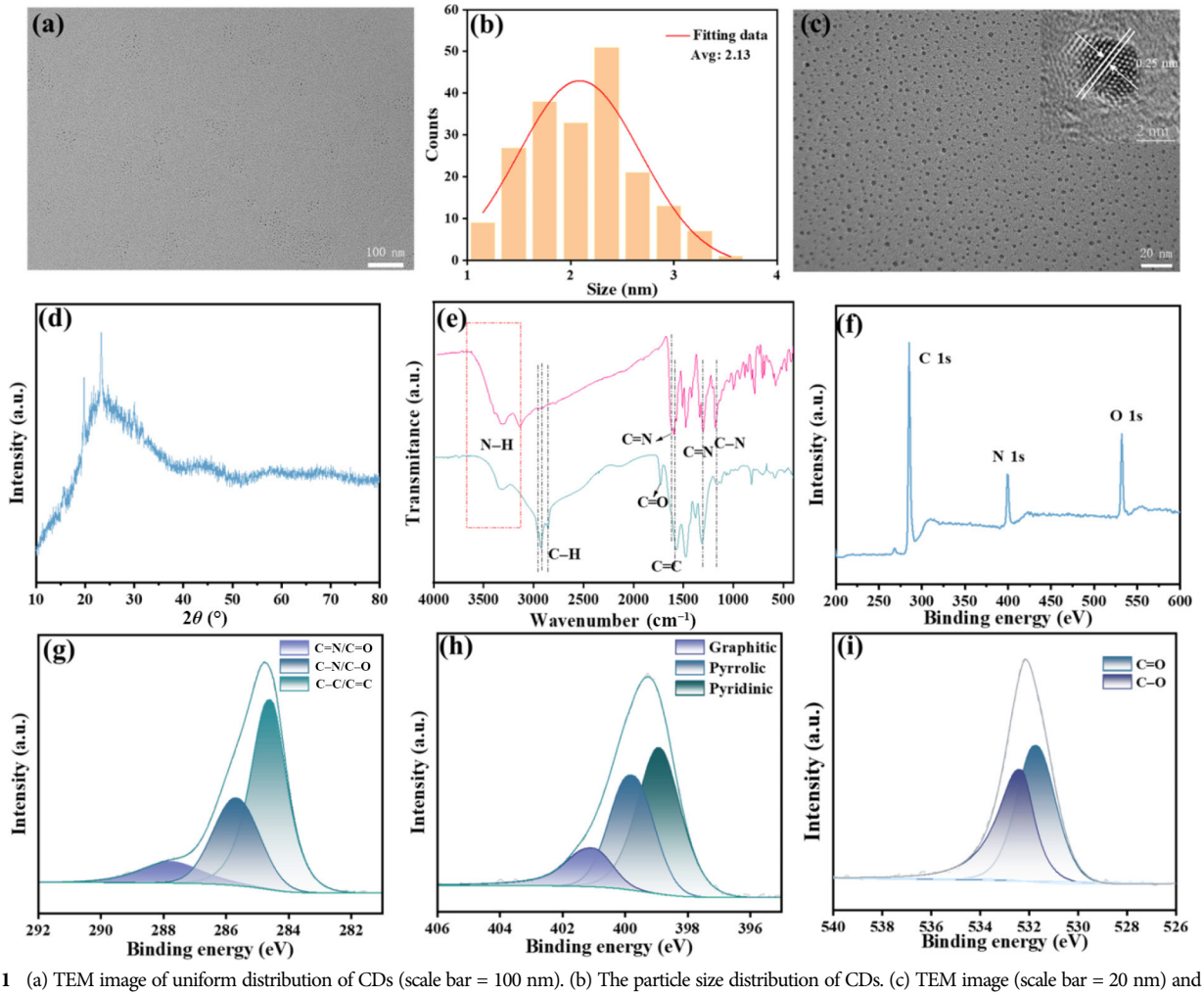

Figure 1 (a) TEM image of uniform distribution of CDs (scale bar = 100 nm). (b) The particle size distribution of CDs. (c) TEM image (scale bar = 20 nm) and (inset) high-resolution TEM image of CDs. (d) XRD pattern of CDs. (e) FT-IR spectra of CDs (bottom) and NR (top). (f) XPS spectrum of CDs. High-resolution XPS spectra of (g) C 1s, (h) N 1s, and (i) O 1s of CDs.

groups [36]. To investigate the chemical bond forms of C, N, and O elements in CDs, high-resolution XPS analysis was performed for fitting. Figure 1(g) illustrates the high-resolution XPS spectrum of C 1s, which can be divided into three small peaks located at approximate 284.8, 285.9, and 287.7 eV. These peaks can be attributed to the presence of C=C/C–C, C–O/C–N, and C=O groups, respectively [37, 38]. Similarly, the high-resolution XPS spectrum of N 1s (Fig. 1(h)) can be decomposed into three peaks near 398.5, 399.5, and 401.2 eV, attributed to pyridine N, pyrrole N, and graphite N, respectively [28, 39, 40]. Figure 1(i) displays the high-resolution XPS spectrum of O 1s, which can be divided into two peaks located near 531.1 and 532.5 eV, corresponding to C=O and C–O bonds, respectively [37, 41]

The synthesized CDs showed bright yellow-green fluorescence in aqueous solution with a photo-quantum yield of 15.13% under neutral conditions (Fig. S1 in the Electronic Supplementary Material (ESM)). And these CDs have good stability (Fig. S2 in the ESM). It is worth noting that EDA exhibits strong alkalinity due to the introduction of more amino groups into the CDs system as one of the precursors. As the pH decreased from 10 to 1, the fluorescence changed regularly from green to red, as shown in Fig. 2(a). The spectrum measurements indicate that the emission peak center of the CDs shifts from 522 to 583 nm, exhibiting a relatively linear change (Fig. 2(b)). The position of the emission peak was linearly fitted to the function $y = 6.7x + 592.8$, demonstrating good adaptability (Fig. 2(c)). Additionally, cyclic tests were conducted on the emission wavelengths of CDs at pH levels ranging from 10 to 1 (Fig. S3 in the ESM). The experimental results indicate that there was no significant change in the emission wavelengths of CDs at pH 10 and pH 1 in the green wavelength band after 10 cycles. However, the emission peak at the wavelength end of the red light shows a small blue shift, which may be due to multiple cycles causing the CDs solution to become diluted. These findings indicate that CDs have good recyclability in pH detection. To investigate the color-changing mechanism of the CDs, we examined their luminescence. For research convenience, we analyzed three groups of CDs with significant differences in emission wavelengths. These CDs were named as green CDs (G-CDs), yellow CDs (Y-CDs), and red CDs (R-CDs), and had pH values of 11, 6, and 1, respectively. The luminescent centers of the three CDs are located at 522, 552, and 584 nm, respectively. To investigate the reason for the red shift of CDs luminescence caused by pH value, we tested the emission spectra of CDs under different wavelength excitation. The results in Fig. 2 show that new emission peaks appear near 580 nm for G-CDs and Y-CDs as the excitation wavelength increases (Figs. 2(d) and 2(e)). For R-CDs, a new emission peak around 605 nm appeared in addition to the intrinsic peak located near 580 nm (Fig. 2(f)). This indicates that the CDs may have two luminescent centers.

To analyze the excitation and emission peaks of the CDs, we conducted a Gaussian peak analysis. Figures 3(a)–3(c) show that G-CDs and Y-CDs have additional peaks near 580 nm, while R-CDs have peaks near 610 nm, in addition to their main emission peaks. This confirms that CDs have multiple emission centers. Excitation spectra reveal that G-CDs have excitation peaks at 320 and 400 nm (Fig. 3(a)), while Y-CDs have an additional excitation peak at 470 nm (Fig. 3(b)). New excitation peaks were observed at 470 and 540 nm for R-CDs (Fig. 3(c)). It is important to note that the excitation peak at 400 nm is significantly weakened in R-CDs. We tested the absorption spectra of the CDs. UV–vis light absorption can be observed with a strong absorption peak located near 280 nm, which is the absorption of π–π* electron transitions from the sp^2 structure of the carbon core (Figs. 3(d)–3(f)) [42, 43]. Functional groups such as C=N/C=O on the surface of CDs cause visible light absorption between 400 and 600 nm [42, 43]. It is interesting that when CDs change from alkaline to acidic, the

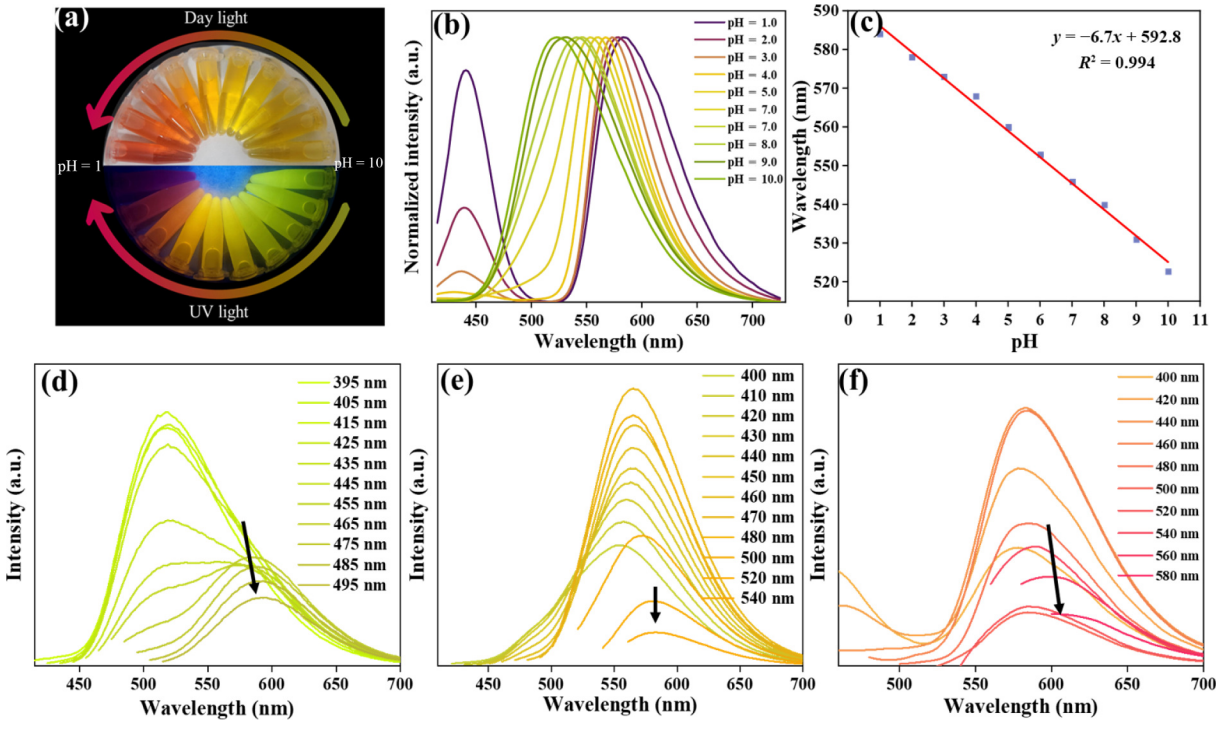

Figure 2 (a) Optical photos of CDs at different pH levels. (b) Emission spectra of CDs at different pH levels. (c) Fitting plots of emission peak positions of CDs at different pH values. (d)–(f) Emission spectra of CDs (G-CDs, Y-CDs, and R-CDs, respectively) at different excitation wavelengths.

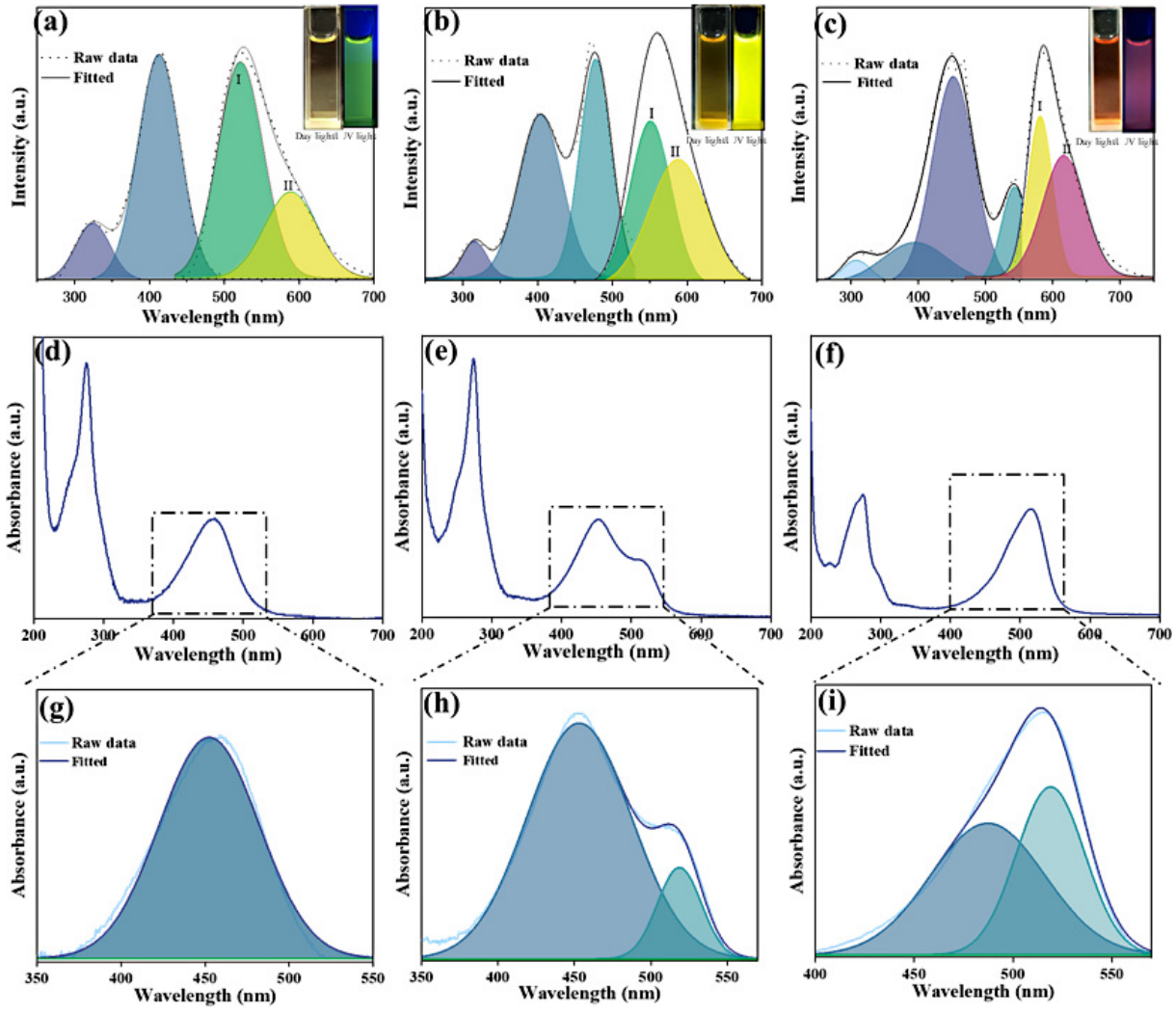

Figure 3 The fitted excitation-emission spectra of (a) G-CDs, (b) Y-CDs, and (c) R-CDs (the insets show CDs under daylight and UV light, respectively). Absorption spectra after (d) G-CDs, (e) Y-CDs, and (f) R-CDs. The fitted absorption spectra of (g) G-CDs, (h) Y-CDs, and (i) R-CDs.

absorption peak in the visible light band shows a significant red shift (Figs. 3(g)–3(i)), which leads to an increase in the self-absorption of CDs in the long wavelength region, resulting in enhanced emission. At the same time, we observed that the absorption from CDs and carbon core weakened compared to the process of changing from alkaline to acidic, indicating the transfer of absorption from the core state to the surface state of CDs.

NR is an acid-base indicator that is highly sensitive to both acid and base. It exhibits a wide absorption band with a peak of 452 nm in alkaline aqueous solutions, which shifts to 535 nm under acidic conditions. Its fluorescence, characterized by a signal peak at 637 nm, is independent of the pH value in water [24, 25]. Furthermore, NR is highly sensitive to environmental polarity and the formation of hydrogen bonds. It is speculated that certain emission centers may be associated with the luminescence of NR. To test this hypothesis, we examined the excitation and emission spectra of NR under the same pH conditions as G-CDs, Y-CDs, and R-CDs. As shown in Figs. S4(a)–S4(c) in the ESM, NR emits red light in various environments. The emission peaks of NR are located at 623 nm at pH = 10, and near 630 nm at pH = 6 and pH = 1, respectively, consistent with literature reports. It is found that the main excitation peak of NR under alkaline conditions is located at 470 nm. A new excitation peak at 540 nm appears in the CDs when transitioning from alkaline to acidic conditions, and this peak increases with acidity. The synthesized CDs also exhibit excitation peaks around 470 and 540 nm when the acidity is enhanced. Additionally, NR's absorption in the visible light band varies depending on the alkalinity and acidity levels, as shown in Figs. S4(d) and S4(e) in the ESM. This absorption pattern is similar to that of CDs in alkalinity and acidity, indicating that the CDs retain the structural characteristics of the precursor.

Absorption in the visible band usually originates from the surface groups of the CDs, which suggests that the CDs surface was incompletely carbonized during the synthesis process and retained some NR properties, resulting in a change in absorbance. It is important to note that a significant red shift in the absorption of NR was found in the long wavelength compared to Y-CDs and R-CDs. This shift is caused by the interaction of NR with the local environment on the surface or inside of the carbon core. On the other hand, the CDs exhibit a later transition from 450 to 520 nm absorption, which is highly likely due to the carbonized matrix altering their proton balance.

The fluorescence decay curves in Fig. S5 in the ESM display that the lifetime of the CDs remains relatively stable at pH 4–8, but

decreases at pH 1–3 and 9–10. At pH 4–8, no major changes were detected. However, at a pH between 1 and 3, the fluorescence lifetime significantly reduces, possibly due to emission quenching caused by excessive addition of acid reagents. It is worth noting that NR solutions exhibit two coexisting luminescent states, as reported extensively [25, 44]. The fluorescence decay was fitted using a bi-exponential model, and the resulting data is presented in Table S1 in the ESM. At pH 8–10, the amplitude (A_1) of lifetime τ_1 is large, but as pH decreases, the amplitude of τ_1 decreases significantly. At pH 1–3, the amplitude of τ_1 increases, but the lifetime τ_1 decreases compared to the lifetime τ_2. This indicates that the emission in the short-wave region weakens with decreasing pH. In addition, FT-IR studies were carried out on G-CDs, Y-CDs, and R-CDs. Figure S6 in the ESM indicates that R-CDs exhibited characteristic $-NH^{3+}$ functional groups when in an acidic environment, suggesting likely protonation of the amino functional groups on the surface of the CDs. Previous reports suggest that protonation may be a significant factor in the red shift of CDs luminescence [37].

Based on the provided analysis, the possible luminescence mechanism of CDs can be speculated and described in Scheme 2. We calculated the absorption and emission energy level changes of the CDs in different pH states by the equation $E_g^{opt} = 1240/\lambda_{edge}$ [45–48]. By comparing the emission, excitation, and absorption spectra of the CDs and NR, we found that there is a certain similarity between the excitation and absorption spectra of the two, which may be because the characteristic functional groups of the NR precursor have not been completely carbonized and are retained on the surface of the CDs. Similar to NR, CDs exhibit two different surface luminescence states. These states can be categorized into surface state I, which emits shorter wavelengths, and surface state II, which emits longer wavelengths. When the pH of the CDs solution changes from basic to acidic, the surface functional groups are protonated. This leads to an increase in absorption in the long wavelength region and some red shift of the emission [49]. As the pH decreases further, the short-wavelength emission of the CDs (state I) is gradually weakened by acid burst, as verified by the significant decrease in lifetime τ_1. At this point, the surface functional group of CDs continues to protonate, and the amino structure of the protonated form introduces several n-orbital energy levels between the π and π* transitions, which reduces the gap distance of the photon transitions and induces red fluorescence from CDs, leading to an enhanced emission share of state II with a luminescence red shift [50].

Gelatin is a biomacromolecule that is prepared by thermally denaturing collagen. It possesses good biocompatibility, temperature sensitivity, water solubility, adhesion, and cost-effectiveness. At temperatures above the upper critical solution temperature, which is approximately 40 °C, gelatin has a random coil structure in solution. The addition of high concentrations of $(NH_4)_2SO_4$ to the solution decreases the solubility of gelatin, resulting in its precipitation, a phenomenon known as the "salting out" effect [51]. After being soaked in the $(NH_4)_2SO_4$ solution, the hydrogel filaments can be bundled together, resulting in a significant improvement in their mechanical properties [52]. SEM tests were carried out, as shown in Fig. S7(a) in the ESM, the CDs@hydrogel shows a layered structure and the layers are connected by a porous structure. Figure S7(b) in the ESM shows the FT-IR absorption spectrum of CDs@hydrogel, and it can be seen that CDs@hydrogel has an abundant hydroxyl structure. In addition, we also tested the mechanical properties, and the stress–strain curves showed that the tensile strength of CDs@hydrogel was about 4 MPa. More noteworthy than the tensile strength is the elongation, and the maximum elongation of CDs@hydrogel was about 450%, which indicates that the hydrogel has good tensile properties (Fig. S7(c) in the ESM). It is also worth mentioning that the gelatin and CDs, which are rich in hydrophilic groups, can stabilize a large number of water molecules, which helps to create artificial ion migration channels for the rapid movement of various components in human sweat, thus making the composite film highly responsive to pH stimuli. We tested its surface hydrophilicity and results showed that complete spreading was achieved when a water droplet was dropped on the hydrogel after 1 s (Fig. S7(d) in the ESM).

In addition, CDs@hydrogel still showed excellent pH

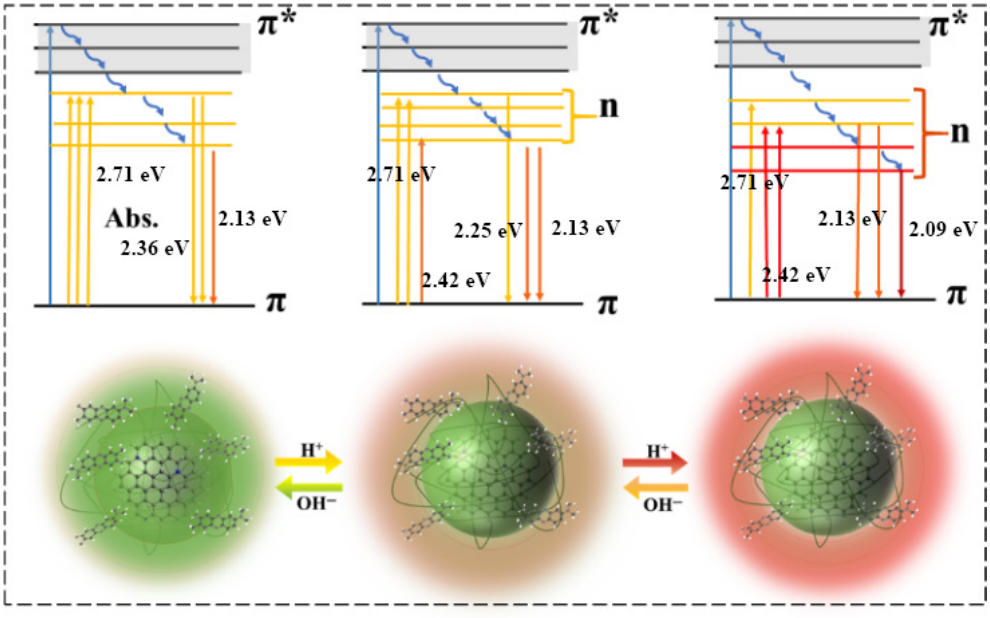

Scheme 2 Schematic diagram of pH sensitivity mechanism of CDs.

discoloration ability. Figure 4(a) displays the optical photographs of CDs@hydrogel at different pH, and it can be seen that the hydrogel showed a significant color change when the pH was changed from 10 to 1. Figure 4(b) shows the change of the hydrogel emission spectra, which can be linearly fitted. It is found that the emission peak positions showed a good linear correlation with pH (Fig. 4(c)). At the same time, we performed a pH cycling test and found that the emission peak positions of the CDs did not change significantly within 20 cycles (Fig. 4(d)). The apparent change in hydrogel color allowed us to use the hydrogel for easier and faster visualization of pH sensing. We took photos with a smart phone and extracted the red, green, and blue (RGB) values of the hydrogel at different pH through software, and we found that the R/G values showed a good non-linear correlation (Fig. 4(e)), which allows us to identify the pH of the solution conveniently through a smart phone.

Due to the good stretching properties of the hydrogel, which has been widely used in the field of sensing, we found that due to the addition of CDs the electrical conductivity of hydrogel has been improved well, and the conductivity changed from 0.1 to 1.2 mS/cm. Therefore, we can try to apply CDs@hydrogel as strain sensors. The strain sensor is assembled by connecting two electrodes to both sides of the hydrogel. The applied stretch causes a change in the cross-sectional area of the hydrogel, which in turn causes a change in its resistance. Upon application of voltage, deformation of the hydrogel leads to a linear resistance change, which facilitates sensitive capture of body movements. The periodic resistance changes during stretching and deformation recovery were found to be stable and reproducible through testing (Fig. 5(a)), demonstrating its potential for application as a strain sensor. By adhering the strain sensor to skin, the hydrogel can be deformed with body movement, leading to orderly changes in resistance, which can be used to detect body movement (Figs. 5(b)–5(e)). We tested different degrees of bending of the knuckle and elbow joints and found that the sensor exhibited different resistance changes for different bends, and also showed sensitive sensing of cyclic changes in the knee and wrist joints. To further test its ability to detect small movements, the strain sensor was integrated into the throat of a volunteer to detect the process of swallowing water (Fig. 5(f)), and the motion of the volunteer swallowing saliva could be sensitively detected. This demonstrates the promising application of CDs@hydrogel as a motion sensor.

Sweat, as an inevitable product during the exercise process, is known to have a strict pH distribution between 4 and 8, which is driven by lactic acid secreted by the exercising muscles [3]. Therefore, the intelligent detection of pH changes is important for reflecting the physiological information of human health. It has been verified through previous experiments that CDs@hydrogel has a promising application in pH sensing and can be used as a convenient visual detection. Therefore, we combined these two functions as a tool for human motion detection and sweat pH detection during exercise. As shown in Fig. 6, we verified the feasibility of CDs@hydrogel for motion sensing and pH sensing by lifting a dumbbell as an action. We conducted a 10 min continuous test, as shown in Fig. 6(b), and the CDs@hydrogel sensor showed a sensitivity due to the motion action in the 10 min test. Figure 6(c) shows a zoomed-in detail, where the rate of change of the resistance in different degrees represents the magnitude of the movement, by which we can monitor the completion of the movement during the exercise. Figure 6(d) shows the change in fluorescence color of CDs@hydrogel before and after the exercise. By extracting the R, G and B values, we can see that the R/G values before and after the exercise are 0.92 and 1.01, respectively. Finally, we conducted the statistics of the whole exercise process, as shown in Fig. 6(e), the whole exercise process lasted 630 s, in which the length of the exercise was 398 s and the length of the rest was 232 s, and the total number of times of lifting the dumbbells was 150, which could be

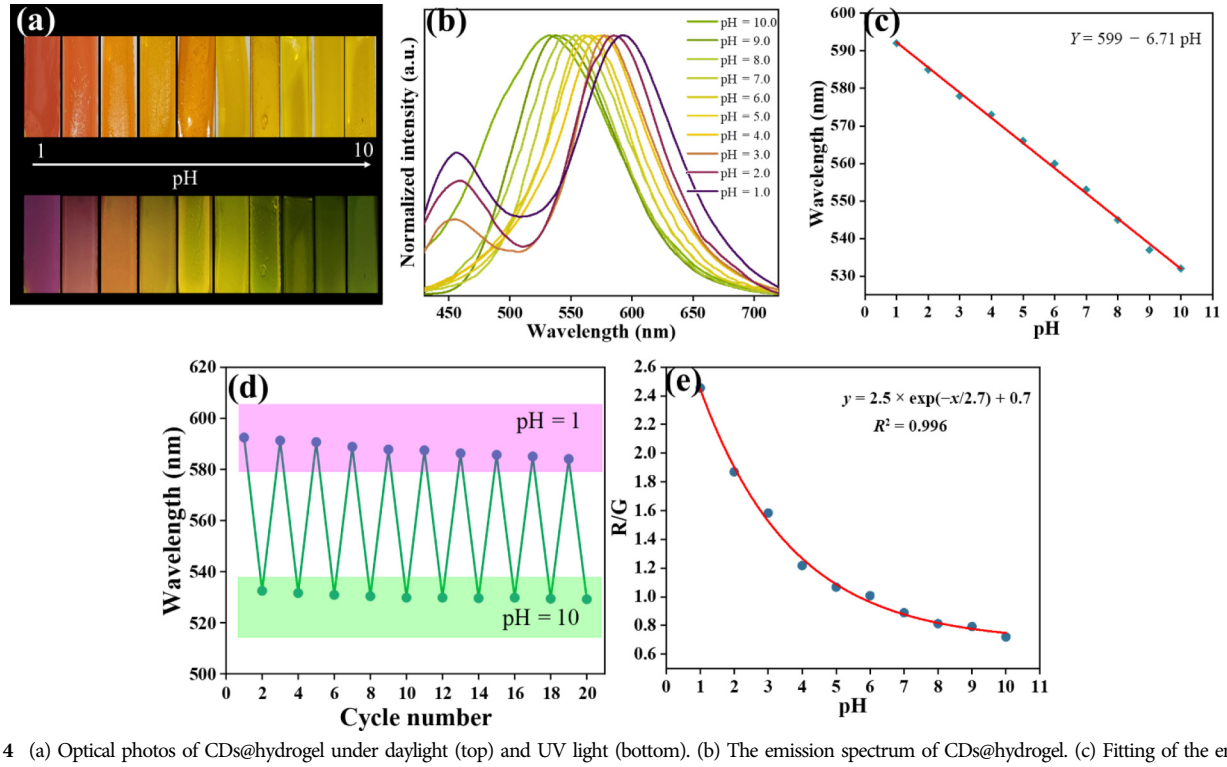

Figure 4 (a) Optical photos of CDs@hydrogel under daylight (top) and UV light (bottom). (b) The emission spectrum of CDs@hydrogel. (c) Fitting of the emission wavelength of CDs@hydrogel. (d) The cycle of CDs@hydrogel wavelength at pH 10 and pH 1. (e) Fitted plots of G/R values at different pH.

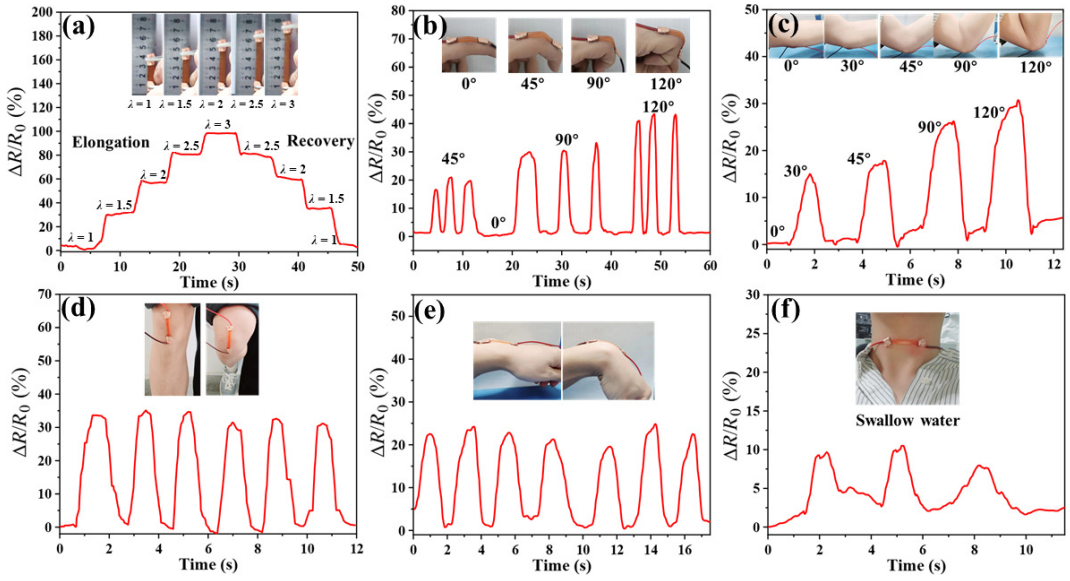

Figure 5 Human motion sensing. (a) Resistance change of strain sensor. (b) Finger bending sensing. (c) Arm bending sensing. (d) Knee joint bending sensing. (e) Wrist bending sensing. (f) Swallowing saliva sensing.

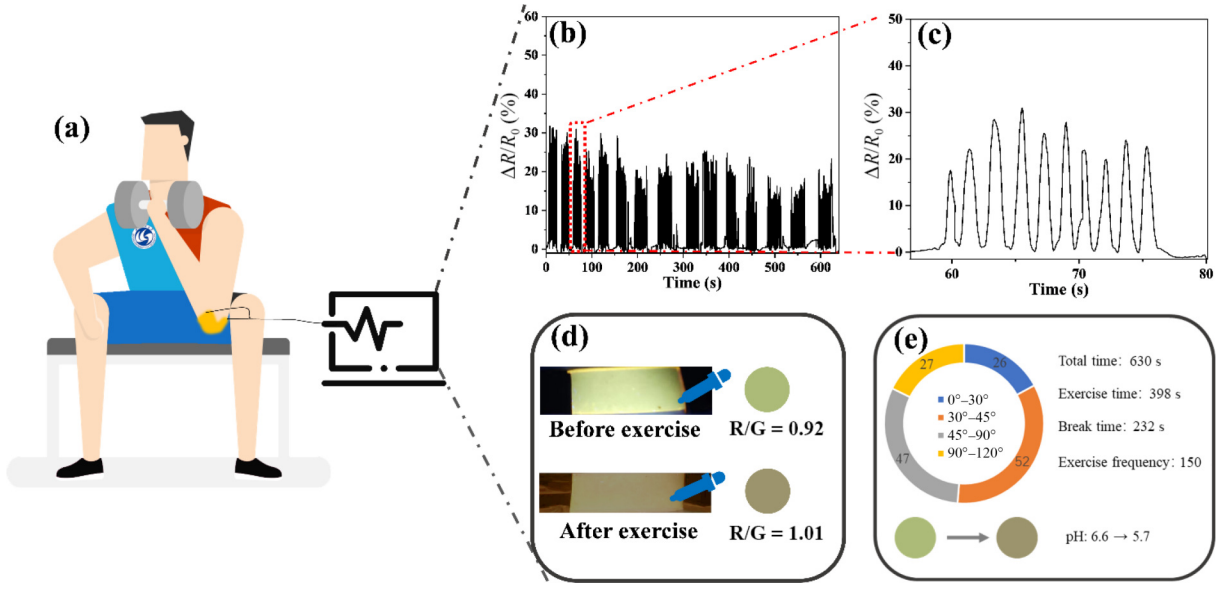

Figure 6 (a) Schematic diagram of CDs@hydrogel motion sensing. (b) CDs@hydrogel for real motion sensing. (c) Local enlargement of (b). (d) Fluorescence photo of CDs@hydrogel before and after motion. (e) Summary of motion data.

obtained by the resistance rate of change. Secondly, our test results in Fig. 5(c) divided the range of resistance rate of change values into 4 groups, corresponding to 4 different elbow flexion angle ranges, so that we can get the number of exercises with different elbow flexions (pie chart in Fig. 6(e)). Finally, by substituting the R/G values into the fitting equation in Fig. 4(e), we can get the pH change from 6.6 to 5.7 during the exercise process. By testing the actual exercise, we have verified the feasibility of CDs@hydrogel for exercise detection and sweat pH monitoring during the process. Meanwhile, based on this we can get a large amount of motion data, which demonstrates that CDs@hydrogel has great application prospects in the field of motion sensing.

4 Conclusions

In summary, we have reported a new type of pH-sensitive CDs. The CDs not only responded to pH in intensity, but their emission wavelength also changed linearly with pH. We found that a continuous change of the CDs from green to red light could be achieved only by changing the pH of the CDs. A series of characterization analyses revealed that this color-changing effect originates from its two-surface-state emission. This property allows us to accurately determine the pH of the solution by measuring the emission wavelength of the CDs, thus avoiding some of the problems in conventional pH determination methods, such as the inaccuracy of the measurement results and the complexity of the operation. In addition, we also found that the change in the emission wavelength of such CDs makes an obvious change in their luminescence color, and we can directly observe the change in the color of the solution with the naked eye, thus realizing the visual detection of the pH of the solution. We further combined the pH-sensitive CDs with hydrogel to prepare a novel pH-sensitive luminescent hydrogel composite. This hydrogel composite not only inherited the pH sensitivity of the CDs but also made the hydrogel

conductive due to the conductivity of the CDs. This allows us to use this hydrogel for motion sensing and sweat pH detection in the human body. Overall, our study opens up new possibilities for multifunctional applications of the CDs.

Electronic Supplementary Material: Supplementary material (Figs. S1–S7 and Table S1) is available in the online version of this article at https://doi.org/10.26599/NR.2025.94907180.

Data availability

All data needed to support the conclusions in the paper are presented in the manuscript and the Electronic Supplementary Material. Additional data related to this paper may be requested from the corresponding author upon request.

Acknowledgements

This work was supported by the National Natural Science Foundation of China (No. 21774098).

Declaration of competing interest

All the contributing authors reports no conflict of interests in this work.

Author contribution statement

J. J. C.: Methodology, investigation, visualization, formal analysis, writing – original draft. H. J. H.: Investigation, data curation, software, formal analysis, visualization, validation, writing – original draft. J. R. L.: Writing – review & editing. J. F. L.: Writing – review & editing. X. G.: Conceptualization, supervision, funding acquisition, project administration, writing – review & editing. All the authors have approved the final manuscript.

Use of AI statement

None.

References

[1] Zhang, L.; Hao, Y. M.; Liu, Y.; Dong, Y. P.; Chen, Z. X.; Dong, W. J.; Zhao, Z. H.; Hu, Q.; Dong, C.; Gong, X. J. Nickel doping: Improving the optical properties of carbon dots and increasing the sensitivity for detecting pH and water. *J. Alloys Compd.* **2024**, *976*, 173131.

[2] Chatzimitakos, T. G.; Kasouni, A. I.; Stalikas, C. D. Multi-purpose nitrogen and phosphorous codoped carbon nanodots for fluorescence-based sensing and bioimaging. *Chem. Eng. J.* **2023**, *476*, 146686.

[3] Tao, X. Y.; Liao, M.; Wu, F. X.; Jiang, Y. H.; Sun, J. P.; Shi, S. H. Designing of biomass-derived carbon quantum dots@polyvinyl alcohol film with excellent fluorescent performance and pH-responsiveness for intelligent detection. *Chem. Eng. J.* **2022**, *443*, 136442.

[4] Ci, Q.; Wang, Y. Y.; Wu, B.; Coy, E.; Li, J. J.; Jiang, D. Y.; Zhang, P. F.; Wang, G. C. Fe-doped carbon dots as NIR-II fluorescence probe for *in vivo* gastric imaging and pH detection. *Adv. Sci* **2023**, *10*, e2206271.

[5] Durrani, S.; Yang, Z. H. Y.; Zhang, J.; Wang, Z. H.; Wang, H. Y.; Durrani, F.; Wu, F. G.; Lin, F. M. Nucleus-targeting pH-responsive carbon dots for fast nucleus pH detection. *Talanta* **2023**, *252*, 123855.

[6] Wang, R. X.; Wang, X. F.; Sun, Y. M. One-step synthesis of self-doped carbon dots with highly photoluminescence as multifunctional biosensors for detection of iron ions and pH. *Sens. Actuators B: Chem.* **2017**, *241*, 73–79.

[7] Bei, Y. Y.; Arkin, K.; Zheng, Y. X.; Ma, X. S.; Zhao, J.; Jin, H. M.; Shang, Q. K. Construction of a ratiometric fluorescent probe for visual detection of urea in human urine based on carbon dots prepared from Toona sinensis leaves and 5-carboxyfluorescein. *Anal. Chim. Acta* **2023**, *1240*, 340733.

[8] Liu, W. J.; Li, C.; Sun, X. B.; Pan, W.; Wang, J. P. Carbon-dot-based ratiometric fluorescent pH sensor for the detections of very weak acids assisted by auxiliary reagents that contribute to the release of protons. *Sens. Actuators B: Chem.* **2017**, *244*, 441–449.

[9] Shangguan, J. F.; He, D. G.; He, X. X.; Wang, K. M.; Xu, F. Z.; Liu, J. Q.; Tang, J. L.; Yang, X.; Huang, J. Label-free carbon-dots-based ratiometric fluorescence pH nanoprobes for intracellular pH sensing. *Anal. Chem.* **2016**, *88*, 7837–7843.

[10] Cui, F. C.; Xi, L. Q.; Wang, D. F.; Ren, L. K.; Tan, X. Q.; Li, X. P.; Li, J. R.; Li, T. T. Advanced in carbon dot-based hydrogels for antibacterial, detection and adsorption. *Coord. Chem. Rev.* **2023**, *497*, 215457.

[11] Zhang, Y. W.; Dai, Y.; Xia, F.; Zhang, X. J. Gelatin/polyacrylamide ionic conductive hydrogel with skin temperature-triggered adhesion for human motion sensing and body heat harvesting. *Nano Energy* **2022**, *104*, 107977.

[12] Chen, J. Y.; Liu, F. F.; Abdiryim, T.; Liu, X. An overview of conductive composite hydrogels for flexible electronic devices. *Adv. Compos. Hybrid Mater.* **2024**, *7*, 35.

[13] Zhu, J. B.; Tao, J. C.; Yan, W.; Song, W. X. Pathways toward wearable and high-performance sensors based on hydrogels: Toughening networks and conductive networks. *Natl. Sci. Rev.* **2023**, *10*, nwad180.

[14] Wang, Y. J.; Lv, T. J.; Yin, K. Y.; Feng, N.; Sun, X. F.; Zhou, J.; Li, H. G. Carbon dot-based hydrogels: Preparations, properties, and applications. *Small* **2023**, *19*, e2207048.

[15] Xu, Q.; Wu, Z. J.; Zhao, W.; He, M. P.; Guo, N.; Weng, L.; Lin, Z. P.; Taleb, M. F. A.; Ibrahim, M. M.; Singh, M. V. et al. Strategies in the preparation of conductive polyvinyl alcohol hydrogels for applications in flexible strain sensors, flexible supercapacitors, and triboelectric nanogenerator sensors: An overview. *Adv. Compos. Hybrid Mater.* **2023**, *6*, 203.

[16] Wang, Z. W.; Wei, H.; Huang, Y. J.; Wei, Y.; Chen, J. Naturally sourced hydrogels: Emerging fundamental materials for next-generation healthcare sensing. *Chem. Soc. Rev.* **2023**, *52*, 2992–3034.

[17] Kurian, A. G.; Singh, R. K.; Sagar, V.; Lee, J. H.; Kim, H. W. Nanozyme-engineered hydrogels for anti-inflammation and skin regeneration. *Nano-Micro Lett.* **2024**, *16*, 110.

[18] Taboada, G. M.; Dahis, D.; Dosta, P.; Edelman, E.; Artzi, N. Sprayable hydrogel sealant for gastrointestinal wound shielding. *Adv. Mater.* **2024**, *36*, 2311798.

[19] Daly, A. C.; Riley, L.; Segura, T.; Burdick, J. A. Hydrogel microparticles for biomedical applications. *Nat. Rev. Mater.* **2019**, *5*, 20–43.

[20] Hu, L. X.; Chee, P. L.; Sugiarto, S.; Yu, Y.; Shi, C. Q.; Yan, R.; Yao, Z. Q.; Shi, X. W.; Zhi, J. C.; Kai, D. et al. Hydrogel-based flexible electronics. *Adv. Mater.* **2023**, *35*, 2205326.

[21] Prince, E.; Kumacheva, E. Design and applications of man-made biomimetic fibrillar hydrogels. *Nat. Rev. Mater.* **2019**, *4*, 99–115.

[22] Li, Z. K.; Lu, J. J.; Ji, T.; Xue, Y. M.; Zhao, L. B.; Zhao, K.; Jia, B. Q.; Wang, B.; Wang, J. X.; Zhang, S. M. et al. Self-healing hydrogel bioelectronics. *Adv. Mater.* **2024**, *36*, 2306350.

[23] Sui, B.; Li, Y. F.; Yang, B. Nanocomposite hydrogels based on carbon dots and polymers. *Chin. Chem. Lett.* **2020**, *31*, 1443–1447.

[24] Sousa, C.; Sá E Melo, T.; Gèze, M.; Gaullier, J. M.; Mazière, J. C.; Santus, R. Solvent polarity and ph effects on the spectroscopic properties of neutral red: Application to lysosomal microenvironment probing in living cells. *Photochem. Photobiol.* **1996**, *63*, 601–607.

[25] Madonia, A.; Minervini, G.; Terracina, A.; Pramanik, A.; Martorana,

V.; Sciortino, A.; Carbonaro, C. M.; Olla, C.; Sibillano, T.; Giannini, C. et al. Dye-derived red-emitting carbon dots for lasing and solid-state lighting. *ACS Nano* **2023**, *17*, 21274–21286.

[26] Li, J. R.; Chen, J. C.; Zhao, X. J.; Vomiero, A.; Gong, X. High-loading of organosilane-grafted carbon dots in high-performance luminescent solar concentrators with ultrahigh transparency. *Nano Energy* **2023**, *115*, 108674.

[27] Wu, M. Y.; Li, J. R.; Wu, Y. Z.; Gong, X.; Wu, M. Design of a synthetic strategy to achieve enhanced fluorescent carbon dots with sulfur and nitrogen codoping and its multifunctional applications. *Small* **2023**, *19*, 2302764.

[28] Li, J. R.; Zhao, H. G.; Zhao, X. J.; Gong, X. Boosting efficiency of luminescent solar concentrators cusing ultra-bright carbon dots with large Stokes shift. *Nanoscale Horiz.* **2022**, *8*, 83–94.

[29] Chen, J. C.; Zhao, H. G.; Li, Z. L.; Zhao, X. J.; Gong, X. Highly efficient tandem luminescent solar concentrators based on eco-friendly copper iodide based hybrid nanoparticles and carbon dots. *Energy Environ. Sci.* **2022**, *15*, 799–805.

[30] Hu, T. T.; Wen, Z. Q.; Wang, C.; Thomas, T.; Wang, C. X.; Song, Q. J.; Yang, M. H. Temperature-controlled spectral tuning of full-color carbon dots and their strongly fluorescent solid-state polymer composites for light-emitting diodes. *Nanoscale Adv.* **2019**, *1*, 1413–1420.

[31] Jiao, Y.; Liu, Y.; Meng, Y. T.; Gao, Y. F.; Lu, W. J.; Liu, Y.; Gong, X. J.; Shuang, S. M.; Dong, C. Novel processing for color-tunable luminescence carbon dots and their advantages in biological systems. *ACS Sustain. Chem. Eng.* **2020**, *8*, 8585–8592.

[32] Paydar, S.; Feizi, F.; Shamsipur, M.; Barati, A.; Chehri, N.; Taherpour, A.; Jamshidi, M. An ideal ratiometric fluorescent probe provided by the surface modification of carbon dots for the determination of Pb^{2+}. *Sens. Actuators B: Chem.* **2022**, *369*, 132243.

[33] Cai, S.; Li, J. Q.; Sun, P. J.; Tao, J.; Fu, Y. F.; Yang, R.; Li, Z. H.; Qu, L. B. Red emissive carbon dots-based polymer beads for recyclable and ultra-sensitive detection of malachite green in fish tissue. *Sens. Actuators B: Chem.* **2023**, *380*, 133311.

[34] Zhang, X.; Tan, X. Y.; Hu, Y. P. Blue/yellow emissive carbon dots coupled with curcumin: A hybrid sensor toward fluorescence turn-on detection of fluoride ion. *J. Hazard. Mater.* **2021**, *411*, 125184.

[35] Li, T. Z.; Shi, W.; Shuang, E.; Mao, Q. X.; Chen, X. W. Green preparation of carbon dots with different surface states simultaneously at room temperature and their sensing applications. *J. Colloid Interface Sci.* **2021**, *591*, 334–342.

[36] Yan, F.; Li, J. R.; Zhao, X. J.; Gong, X. Unveiling unconventional luminescence behavior of multicolor carbon dots derived from phenylenediamine. *J. Phys. Chem. Lett.* **2023**, *14*, 5975–5984.

[37] Zhang, Q.; Wang, R. Y.; Feng, B. W.; Zhong, X. X.; Ostrikov, K. Photoluminescence mechanism of carbon dots: Triggering high-color-purity red fluorescence emission through edge amino protonation. *Nat. Commun.* **2021**, *12*, 6856.

[38] Wu, Y. H.; Li, J. R.; Zhao, X. J.; Gong, X. Nickel-doped carbon dots with enhanced and tunable multicolor fluorescence emission for multicolor light-emitting diodes. *Carbon* **2023**, *201*, 796–804.

[39] Shen, J.; Zheng, X. J.; Lin, L. L.; Xu, H. J.; Xu, G. H. Reaction time-controlled synthesis of multicolor carbon dots for white light-emitting diodes. *ACS Appl. Nano Mater.* **2023**, *6*, 2478–2490.

[40] Li, L.; Li, Y. T.; Ye, Y.; Guo, R. T.; Wang, A. N.; Zou, G. Q.; Hou, H. S.; Ji, X. B. Kilogram-scale synthesis and functionalization of carbon dots for superior electrochemical potassium storage. *ACS Nano* **2021**, *15*, 6872–6885.

[41] Cao, M. Y.; Zhao, X. J.; Gong, X. Ionic liquid-assisted fast synthesis of carbon dots with strong fluorescence and their tunable multicolor emission. *Small* **2022**, *18*, e2106683.

[42] Ru, Y.; Sui, L.; Song, H. Q.; Liu, X. J.; Tang, Z. Y.; Zang, S. Q.; Yang, B.; Lu, S. Y. Rational design of multicolor-emitting chiral carbonized polymer dots for full-color and white circularly polarized luminescence. *Angew. Chem., Int. Ed.* **2021**, *60*, 14091–14099.

[43] Dong, Y. Q.; Pang, H. C.; Yang, H. B.; Guo, C. X.; Shao, J. W.; Chi, Y. W.; Li, C. M.; Yu, T. Carbon-based dots co-doped with nitrogen and sulfur for high quantum yield and excitation-independent emission. *Angew. Chem., Int. Ed.* **2013**, *52*, 7800–7804.

[44] Singh, M. K.; Pal, H.; Bhasikuttan, A. C.; Sapre, A. V. Dual solvatochromism of neutral red. *Photochem. Photobiol.* **1998**, *68*, 32–38.

[45] Yuan, T.; Yuan, F. L.; Sui, L.; Zhang, Y.; Li, Y. C.; Li, X. H.; Tan, Z. A.; Fan, L. Z. Carbon quantum dots with near-unity quantum yield bandgap emission for electroluminescent light-emitting diodes. *Angew. Chem., Int. Ed.* **2023**, *135*, e202218568.

[46] Yuan, F. L.; Wang, Z. B.; Li, X. H.; Li, Y. C.; Tan, Z.; Fan, L. Z.; Yang, S. H. Bright multicolor bandgap fluorescent carbon quantum dots for electroluminescent light-emitting diodes. *Adv. Mater.* **2017**, *29*, 1604436.

[47] Jia, H. R.; Wang, Z. B.; Yuan, T.; Yuan, F. L.; Li, X. H.; Li, Y. C.; Tan, Z. A.; Fan, L. Z.; Yang, S. H. Electroluminescent warm white light-emitting diodes based on passivation enabled bright red bandgap emission carbon quantum dots. *Adv. Sci.* **2019**, *6*, 1900397.

[48] Yuan, F. L.; Wang, Y. K.; Sharma, G.; Dong, Y. T.; Zheng, X. P.; Li, P. C.; Johnston, A.; Bappi, G.; Fan, J. Z.; Kung, H. et al. Bright high-colour-purity deep-blue carbon dot light-emitting diodes via efficient edge amination. *Nat. Photonics* **2020**, *14*, 171–176.

[49] Liu, Y. P.; Guo, C.; Wu, G. F.; Lv, W. J.; Zhou, R. C.; Qiu, W.; Zhou, Y.; Xu, Q.; Xu, C. M.; Niu, Y. C. Uniformly dispersed bismuth metal nano catalyst modified carbon cloth electrode for iron-chromium flow battery. *Nano Research Energy*, in press, https://doi.org/10.26599/NRE.2024.9120135.

[50] Zhang, Q.; Wang, F. Q.; Wang, R. Y.; Liu, J. L.; Ma, Y. P. X.; Qin, X. R.; Zhong, X. X. Activating one/two-photon excited red fluorescence on carbon dots: Emerging $n \rightarrow \pi$ photon transition induced by amino protonation. *Adv. Sci.* **2023**, *10*, e2207566.

[51] Tang, Y. Y.; Xu, Q.; Zhang, X. Y.; Zhu, R. Y.; Zhao, N.; Wang, J. C. Expediting carbon dots synthesis by the active adaptive method with machine learning and applications in dental diagnosis and treatment. *Nano Res.* **2024**, *17*, 10109–10118.

[52] He, Q. Y.; Huang, Y.; Wang, S. Y. Hofmeister effect-assisted one step fabrication of ductile and strong gelatin hydrogels. *Adv. Funct. Mater.* **2018**, *28*, 1705069.